Microporous and Mesoporous Materials 323 (2021) 111230

Contents lists available at ScienceDirect

Microporous and Mesoporous Materials

journal homepage: www.elsevier.com/locate/micromeso

AgY zeolite as catalyst for the selective catalytic oxidation of NH_3

Joaquin Martinez-Ortigosa [a], Christian W. Lopes [a,b], Giovanni Agostini [c], A. Eduardo Palomares [a], Teresa Blasco [a,*], Fernando Rey [a]

[a] Instituto de Tecnología Química, Universitat Politècnica de València - Consejo Superior de Investigaciones Científicas (UPV-CSIC), Avda. de los Naranjos s/n, 46022, Valencia, Spain
[b] Institute of Chemistry, Universidade Federal do Rio Grande do Sul – UFRGS, Av. Bento Gonçalves, 9500, P.O. Box 15003, 91501-970, Porto Alegre, RS, Brazil
[c] ALBA Synchrotron Light Source, Crta. BP 1413, Km. 3.3, Cerdanyola del Vallès, 08290, Spain

ARTICLE INFO

Keywords:
Ag-containing zeolites
Selective ammonia oxidation
In situ XAS
^{109}Ag solid-state NMR

ABSTRACT

Ag-exchanged Y zeolites (Si/Al = 2.5; Ag/Al = 0.30–0.95) have been tested in the NH_3–SCO reaction, the most promising method for the elimination of ammonia emissions, and deeply characterized before and after reaction by using a variety of techniques (XRD, TEM, UV–Vis, ^{109}Ag NMR, XAS spectroscopies). The most active centres for the NH_3–SCO reaction are Ag^0 nanoparticles (NPs) formed under reduction conditions and both activity and selectivity to N_2 increase with the silver loading. The Ag^0 NPs are dramatically modified under reaction conditions, being most of them dispersed resulting in small clusters and even atomically Ag^+ cations, the latter accounting for around half silver atoms. The presence of water into the reaction feed promotes the dispersion and oxidation of silver nanoparticles, but the catalyst performance is only slightly affected. The results are fully consistent with the previously proposed i-SCR mechanism for NH_3–SCO reaction on silver catalysts.

1. Introduction

Ammonia is one of the four main atmospheric pollutants besides NO_x, SO_2 and volatile organic compounds (VOCs), is harmful to human health and has detrimental effects on the environment. Most ammonia emissions come from fertilizes used in agriculture, but it is also released to the atmosphere in biomass burning, fuel combustion and industrial processes [1,2]. In the last years, more strict environmental regulations have intensified the use of selective catalytic reduction units for the depletion of NO_x emission using ammonia in the form of urea as a reducing agent (NH_3-SCR-NO_x) in heavy-duty diesel vehicles, as well as in power plants and other industrial facilities [3,4]. In this process, unreacted ammonia slips to the atmosphere in the exhaust gases, which has motivated an increasing interest in the development of new methods for the elimination of this contaminant. The most promising technology is the selective catalytic oxidation of ammonia (NH_3-SCO) to nitrogen and water using noble metal [5–7] or transition metal ions [8–12] supported on oxides or zeolites as catalysts, being Ag/Al_2O_3 among the most effective [13–17]. Ag/Al_2O_3 is also of interest for the elimination of another atmospheric pollutant, NO_x, as it has been reported to be one of the best catalysts for the SCR-NOx reaction using hydrocarbons as reductants (HC-SCR-NOx), especially when H_2 is added into the reaction feed [18–22].

Ag-zeolites have been extensively studied because of their unique properties with potential applications in different fields such as photochemistry [23,24], as fungicide for bacteriological control [25,26], and catalysis [27–35]. Some of these remarkable properties reside on the formation of small clusters consisting of several atoms, which are stabilized by its confinement in spatially distant cages of the zeolite host hindering the tendency of silver to agglomerate. Some examples of the uses of Ag-zeolites as catalysts are the oxidation of ethylene [32] or VOCS [35], the aromatization of hydrocarbons [33], the HC-SCR-NO_x [28–31], etc. However, in spite of the number of studies on silver-based catalysts, the works concerning the use of Ag-zeolites as catalysts for the NH_3–SCO reaction are very limited [36–38].

The NH_3–SCO reaction is usually accompanied by the formation of other gaseous pollutants due to undesired overoxidation of ammonia giving NO or N_2O [2]. Therefore, besides the activity also the selectivity of the NH_3–SCO reaction is a very important issue to avoid the emission of atmospheric contaminants. Despite the number of investigations carried out, neither the active site nor the mechanism for the NH_3–SCO reaction on silver-based catalysts are clearly established yet. Atomically dispersed Ag^+, neutral or charged silver clusters and metal nanoparticles (NPs) have been identified in Ag-based catalysts, but the species formed

* Corresponding author.
E-mail addresses: tblasco@itq.upv.es, tblasco@itq.upv.es (T. Blasco).

https://doi.org/10.1016/j.micromeso.2021.111230
Received 29 March 2021; Received in revised form 5 May 2021; Accepted 3 June 2021
Available online 8 June 2021

depend on the temperature, the activation atmosphere and the characteristics of the support [13,23,32,36,37,39]. In general, it is assumed that Ag^+ participates in the NH_3–SCO reaction at high temperatures and that small metal NPs are the active sites at low temperatures, whereas the selectivity to N_2 in Ag-zeolites appears to be improved by large particles [13]. Moreover, the presence of Brønsted acid sites on the support has been reported to play a key role in facilitating oxidation and reduction of silver species and stabilizing ammonia as NH_4^+ against deeper oxidation to NO/N_2O [13,14,16,36,37]. Regarding the reaction mechanism, it is generally accepted to occur through the so-called internal SCR (i-SCR), especially for temperatures above 160 °C. According to the i-SCR reaction pathway, the ammonia is first oxidized to NO which is then reduced by unreacted ammonia giving N_2 and water following the NH_3-SCR reaction [2,13–15,36,40]. With this general idea, combination of noble metal based catalysts with transition metal ions active for the SCR reaction can be an alternative for achieving high activity and selectivity in the NH_3–SCO reaction, as reported for Ag/Al_2O_3 doped with copper [41,42].

This work aims at investigating the influence of silver loading and the atmosphere used on the thermal activation of AgNaY zeolites on the species formed and their performance in the NH_3–SCO reaction. The catalytic tests are carried out under dry and more realistic conditions in the presence of water, which is usually a component in the exhaust gas. Our results clearly indicate that Ag^+ sites are not active for the reaction in the whole temperature range, whilst the AgNaY zeolites treated under H_2 are catalytically active. The silver NPs predominant in the reduced AgNaY catalysts are dispersed during the catalytic test to form neutral and/or charged clusters and atomically dispersed Ag^+, which must also participate in the reaction. The characterization of the Ag species is fully consistent with a two steps reaction pathway, involving the proposed i-SCR reaction mechanism for NH_3–SCO reaction.

2. Experimental

2.1. Catalysts preparation

AgNaY zeolites with Ag/Al = 0.95, 0.56, 0.30 molar ratios were prepared by ion exchange of NaY (Si/Al = 2.5) (CBV-100, from Zeolyst) with an aqueous solution of $AgNO_3$ with the desired amount of Ag^+ to get a liquid/solid (m/m) ratio of 100 and mechanically stirred at room temperature for 24 h avoiding light. AgCsY75 zeolite was prepared from a CsY zeolite with a Cs/Al = 0.9 molar ratio obtained by ion exchange of NaY (CBV-100, Zeolyst) with a 1 mol/L aqueous solution of $CsNO_3$ mechanically stirred at room temperature during 24 h seven times. The resulting sample was subsequently exchanged with $AgNO_3$ under the conditions described above to obtain 75% exchange by silver on the zeolite. After the exchange, the samples were filtered out, washed with distilled water and dried at 100 °C overnight. The zeolites are denoted as AgNaY and AgCsY followed by a number that indicates the Ag/Al molar ratio and **_as** for the as-prepared samples. Table 1 shows the chemical composition of the Ag-zeolites with Ag/Al molar ratios ranging from 0.30 to 0.95 and M^+ (Na^+ or Cs^+) resulting (Ag^++ M^+)/Al molar ratios about 1. The X-ray diffraction patterns (not shown) are typical of the FAU type structure, with only small changes in the relative intensity of some diffraction peaks, probably due to modifications in the electronic densities of the *hkl* planes by the presence of Ag^+ at exchange position [43]. The occurrence of Ag^+ is further confirmed by a band at 220 nm in the UV–Vis spectra (not shown) [43,44]. Prior to the catalytic test in the NH_3–SCO reaction, all AgNaY and AgCsY zeolites were reduced at 400 °C for 3.5 h under H_2 using a heating rate of 10 °C·min^{-1} in order to ensure the complete reduction to Ag^0 [38]. The catalytic activity of the AgNaY95 zeolite was also tested on the sample treated under similar conditions but using N_2 (AgNaY95_N_2) or O_2 (AgNaY95_O_2) atmospheres.

Table 1
Chemical composition of Ag-exchanged NaY zeolites. BET and micropore volume (μV) were estimated on the reduced zeolites.

Sample[a]	Ag/Al	M^+/Al[b]	(Ag^+ + M^+)/Al	BET ($m^2 \cdot g^{-1}$)	μV ($cm^3 \cdot g^{-1}$)
NaY[c]	0	1	1	668	0.32
AgNaY30	0.30	0.80	1.10	615	0.23
AgNaY56	0.56	0.52	1.08	606	0.23
AgNaY95	0.95	0.18	1.13	352	0.13
AgCsY75	0.75	0.32	1.07	–	–

[a] Si/Al molar ratio is about 2.5 in all zeolites.
[b] $M^+ = Na^+$ or Cs^+.
[c] NaY is the commercial zeolite CBV-100 used as starting zeolite for all Ag-containing samples.

2.2. Characterization techniques

Morphological and compositional analysis of the Ag-containing zeolites was performed by FESEM using a ZEISS Ultra-55 microscope. The sample powder was deposited in double-sided tape and analyzed without metal covering. The elemental composition and distribution of silver have been determined by using an EDX probe.

X-ray Diffraction (XRD) patterns were measured on a Cubix'Pro diffractometer from Panalytical equipped with an X'Celerator detector and automatic divergence and reception slits (constant irradiated area of 3 mm), operating at 45 kV and 40 mA, and using Cu Kα radiation (λ = 1.542 Å). The XRD patterns of Ag-containing zeolites were compared to reference zeolite Y, Ag^0 and Ag_2O patterns reported in the JCPDS database (files: 00-039-1380, 00-004-0783, 00-012-0793) [45]. The UV–vis spectra of Ag-loaded FAU zeolites were measured on a UV–Vis Cary 5000 spectrometer equipped with a Prying-Mantis® diffuse reflectance accessory. Metallic particle sizes were evaluated by electron microscopy in a JEOL-JEM-2100F microscope operating at 200 kV in transmission mode (TEM). Prior to TEM microscopy analysis, the samples were suspended in isopropanol and submitted to ultrasonication for approximately 1 min. Afterwards, a drop was extracted from the top side and placed on a carbon-coated nickel grid. Metal particle size histograms were generated upon measuring more than 200 particles from several micrographs taken at different positions on the TEM grid. Textural properties of the reduced AgNaY zeolites were determined by measuring N_2 adsorption isotherms at 77 K using a Micromeritics ASAP 2420 volumetric instrument. ^{109}Ag NMR spectra were recorded with a Bruker Avance III HD 400 MHz spectrometer at $\nu_0(^{109}Ag) = 18.6$ MHz using a 7 mm MAS probe at 5 kHz, with a Hahn-Echo sequence with π/2 pulse length of 14 μs and recycle delay of 3 s, using as a secondary reference Ag_3PO_4 ($\delta^{109}Ag$ = 342.5 ppm) [46]. The quantification of the ^{109}Ag NMR spectra was done by using a calibration curve constructed using kaolin samples mixed with different amounts of silver metal (Sigma-Aldrich) and a series of Ag-FAU zeolites with different Ag/Al ratios, quantifying Ag by SEM-EDX.

X-ray absorption spectroscopy (XAS) experiments at the Ag K-edge (25514 eV) were performed at the BL22 (CLÆSS) beamline of ALBA synchrotron (Cerdanyolla del Vallès, Spain) [47]. The white beam was monochromatized using a Si (311) double crystal cooled by liquid nitrogen; harmonic rejection has been performed using Rh-coated silicon mirrors. The spectra were collected in transmission mode by means of the ionization chambers filled with appropriate gases (88% N_2 + 12% Kr for I_0 and 100% Kr for I_1). Samples in the form of self-supported pellets of an optimized thickness (normally to obtain a jump of about 1, approximately), have been located inside an in-house built multipurpose cell described by Guilera [48] allowing *in situ* experiments. Three scans were acquired at each measurement step to ensure spectral reproducibility and good signal-to-noise ratio. The data reduction and extraction of the χ(k) function have been performed using Athena code. EXAFS data analysis has been performed using the Artemis software [49]. Phase and amplitudes have been calculated by FEFF6 code.

2.3. NH_3–SCO experiments

The NH_3–SCO catalytic activity measurements over the AgNaY zeolites were carried out in a fixed-bed quartz tubular reactor using a gas mixture of 500 ppm of NH_3, 7 vol% O_2 and N_2 as a balance, for selected samples a 3% of water vapour was introduced. The total flow rate and the amount of catalyst were 800 mL min^{-1} and 0.25 g respectively, the resulting WHSV for these catalytic experiments was 192.000 mL $h^{-1}g^{-1}$. The outlet gases were analyzed by three on-line detectors: UV-based detector for monitoring the NH_3 (EMX400 Tethys Instruments), an infrared N_2O analyzer (4900 Servomex) and a chemiluminescence detector which allows the quantification of NOx concentration (42C Thermo).

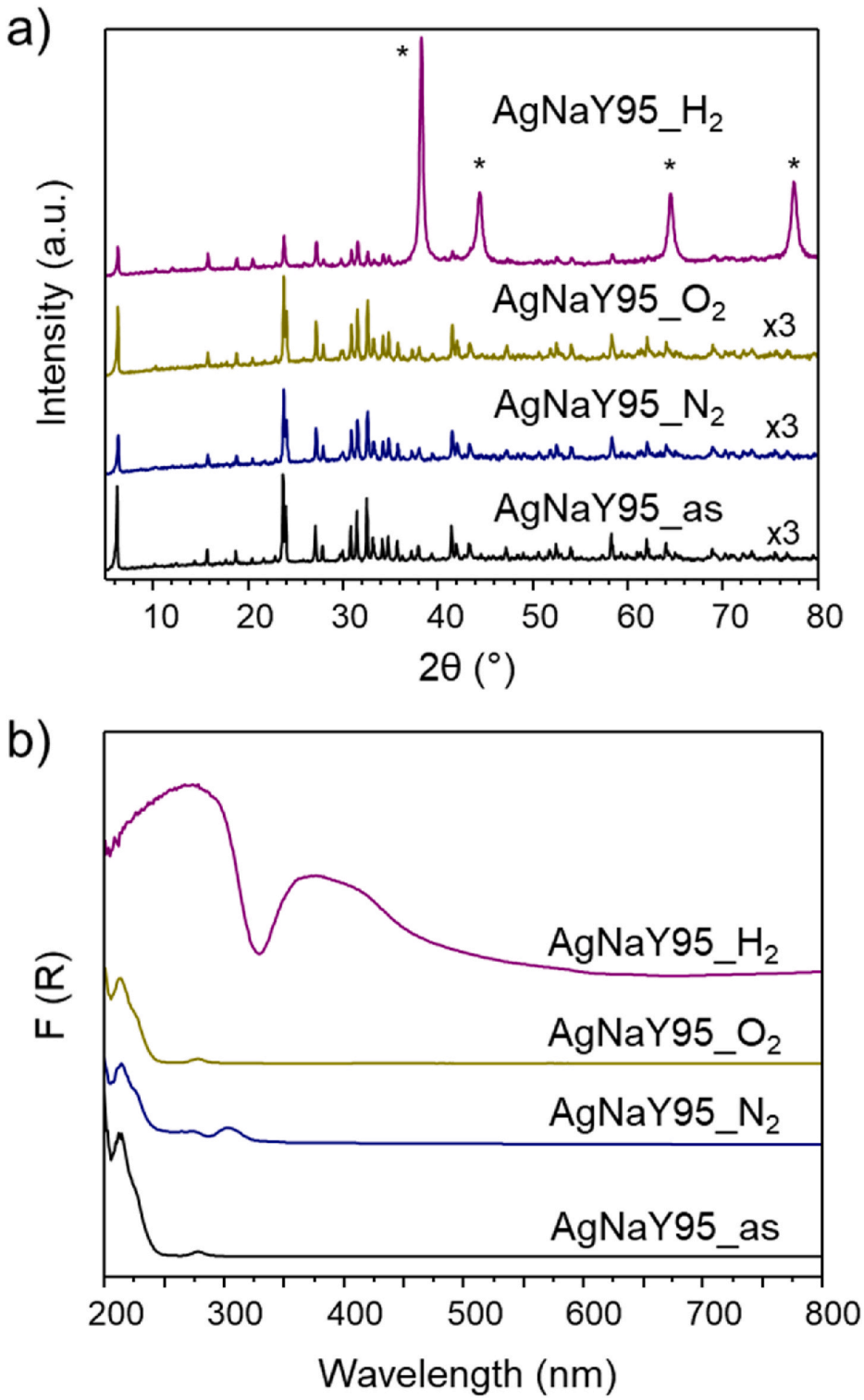

Fig. 1. X-ray diffraction patterns (a) and UV–Vis spectra (b) of the AgNaY95 zeolite as prepared (AgNaY95_as) and treated at 400 °C under O_2 (AgNaY95_O_2), N_2 (AgNaY95_N_2) or H_2 (AgNaY95). (* diffraction peaks of Ag^0 metal).

3. Results

Table 1 shows the chemical composition of the AgNaY zeolites with Ag/Al molar ratio in the range between 0 and 0.95, obtained from an aluminium rich NaY zeolite (Si/Al = 2.5 molar ratio) by chemical exchange. In all zeolites, the framework negative charge due to aluminium is compensated by Na^+ and Ag^+ and therefore, the as-prepared samples do not contain Brønsted acid sites. In order to check the influence of the gas atmosphere used in the thermal activation on the nature of silver species and their catalytic activity, AgNaY95 zeolite was submitted to different treatments and tested in the NH_3–SCO reaction.

Fig. 1 shows the XRD patterns and UV–Vis spectra of the AgNaY95 zeolite as prepared (AgNaY95_as) and heated at 400 °C under O_2 (AgNaY95_O_2), N_2 (AgNaY95_N_2) and H_2 (AgNaY95). The X-ray diffractograms of AgNaY95_as, AgNaY95_O_2 and AgNaY95_N_2 are similar and characteristic of the FAU type zeolite (Fig. 1a). The UV–Vis spectrum of the AgNaY95_as shows a band at 220 nm assigned to the presence of isolated Ag^+, which practically does not change after heating under O_2 (AgNaY95_O_2), while only a very weak band at 310 nm attributed to $[Ag_n]^0$ clusters emerges when N_2 is used (AgNaY95_N_2) [37,43,50] (Fig. 1b). However, when the sample is heated under H_2, the X-ray diffractogram shows intense peaks of Ag^0 (Fig. 1) and the UV–Vis spectrum contains two broad bands (Fig. 1b), one with the maximum at 275 nm attributed to $[Ag_m]^{\delta+}$ and $[Ag_n]^0$ clusters and another one around 400 nm assigned to Ag^0 metal particles [13,37,43,50,51]. The complete reduction of Ag^+ cations (further confirmed by ^{109}Ag MAS-NMR, see below) to silver clusters and NPs in AgNaY95 is necessarily accompanied by the appearance of Brønsted acid sites, needed to compensate the negative charges associated with aluminium isomorphically substituting for silicon in the zeolite framework.

Fig. 2 represents the NH_3 conversion of the AgNaY95_N_2, AgNaY95_O_2 and AgNaY95 zeolites in the NH_3–SCO reaction as a function of the reaction temperature. The AgNaY95 zeolite converts almost 100% NH_3 at 250 °C, indicating that silver NPs are active for the reaction. However, the activity curves of AgNaY95_N_2 and AgNaY95_O_2 are very similar to the thermal reaction (red line), giving 50% NH_3 conversion at 550 °C approximately ($T_{50\%}$ = 550 °C). According to previous studies, the fully exchanged Ag-FAU (Si/Al = 2.5) possesses the 43% of the Ag^+ exposed to the supercavity, indicating that almost half of silver atoms are accessible to reactant molecules [52,53], and then, the catalytic results suggest that Ag^+ is nearly inactive for the reaction. To check if this behaviour is related to the absence of Brønsted acid sites an AgHY (CBV500, zeolyst) zeolite, containing Ag^+ (Ag/Al = 0.30) and acid groups, was activated in O_2 or N_2 atmosphere and also tested in the reaction. As shown in Fig. 2, the NH_3 conversion slightly increases ($T_{50\%}$ ≈ 475 °C), but it is still far from the reduced AgNaY95 zeolite ($T_{50\%}$ ≈ 200 °C) confirming the lack of activity of Ag^+ for this reaction [14].

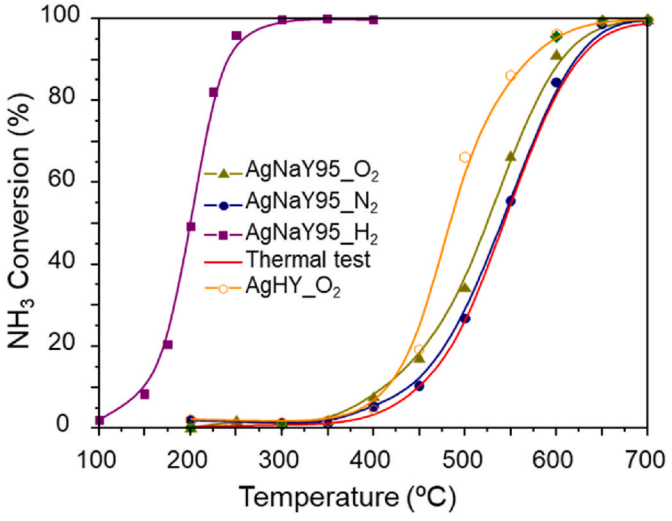

Fig. 2. NH_3 conversion in the NH_3–SCO reaction for the AgNaY95 and AgHY zeolites treated under different atmospheres.

According to these results, the catalytic tests on AgNaY and AgCsY were carried out on the materials reduced under H_2 at 400 °C.

3.1. Influence of silver loading on the characteristic and catalytic performance of AgY zeolites in the NH_3–SCO reaction

The XRD patterns and UV–Vis spectra of all AgNaY zeolites (reduced at 400 °C) with varying amounts of silver are shown in Fig. 3. The X-ray diffractograms display the peaks of zeolite Y and Ag^0 metal. As expected, the relative intensities of the characteristic X-ray reflections of the metallic silver increase with the silver loading (Fig. 3a) [14]. The shape of the UV–Vis spectra of the AgNaY zeolites, shown in Fig. 3b, are slightly different but all display two broad bands with two maxima, one in the 270 nm–300 nm region assigned to positively charged $[Ag_m]^{\delta+}$ and neutral $[Ag_n]^0$ clusters and another in the region 370 nm–425 nm attributed to bulk Ag^0 NPs [37,51].

Transmission electron microscopy (TEM) was used to get information on the size of the metal particles formed on AgNaY30 and AgNaY95 zeolites with the lowest and highest silver loadings, respectively, and the TEM images and the corresponding particle size distribution (PSD) are shown in Fig. 4. Most silver NPs in AgNaY30 are smaller than 20 nm, while AgNaY95 zeolite exhibits a bimodal size distribution with some particles smaller than 10 nm (median at around 4 nm) and the second group of larger particles in the 20–70 nm range (median at around 48 nm). The presence of very small and of large particles could explain the relatively low N_2 adsorption capacity observed for AgNaY95, as they partially blocks the pore openings of the zeolite decreasing the BET area and micropore volume (see Table 1). Due to the lower Ag content, Ag^0 NPs on the surface of AgNaY30 and AgNaY56 zeolites do not block the structural microporosity of the zeolite and BET area and micropore volume are closer to the values found for NaY (CBV100 commercial zeolite, Table 1). Note that the maximum diameter of a sphere which can be allocated within the *fau* supercages is around 1.1 nm, so that the Ag NPs formed upon the H_2 treatment and detected by TEM are placed at the external surface of the zeolite and therefore fully accessible to reactant molecules.

Further information on the degree of aggregation of silver atoms in clusters consisting of few atoms and in NPs was obtained by X-ray Absorption Spectroscopy (XAS). The XANES spectra of the AgNaY30, AgNaY56 and AgNaY95 zeolites and the silver metal foil used as a reference for Ag^0, shown in Fig. 5a, appear at the same energy value, at 25514 eV typical of metallic silver [54]. The XANES spectrum of Ag foil is characterized by two well-defined EXAFS oscillations immediately after the edge (negative and positive peaks at 25538 eV and 25549 eV, respectively) due to the well-arranged *fcc* structure of the metal, where the central Ag atom is coordinated to 12 Ag atoms at 2.86 Å [55]. The intensity of these features contains intrinsically information on the Ag particle size, decreasing the amplitude of the EXAFS oscillation for small particles because of a large fraction of low coordinated atoms on the NPs surface [56]. The spectra of the AgNaY zeolites are similar to the reference foil, indicating that the coordination of a large fraction of Ag atoms in the Ag-zeolites is like in bulk metal [54].

The Fourier transformed (FT) k^3-weighted EXAFS data of all AgNaY zeolites, shown in Fig. 5b, display one intense peak between 2 and 3 Å (not corrected in phase) due to Ag–Ag contribution and three more at longer distances, between 4 and 6 Å, due to higher shells of metallic domains. Both regions have similar intensity and phase than those of silver metal of reference pointing out to the formation of quite ordered silver NPs in AgNaY. As reported in Table 2, the analysis of the first shell of EXAFS data gives, as for metal foil, an average coordination number ($N_{Ag–Ag}$) of 12 and Ag–Ag distances ($R_{Ag\text{-}Ag}$) of approximately 2.86 Å or slightly shorter (within errors). The well-known correlation between

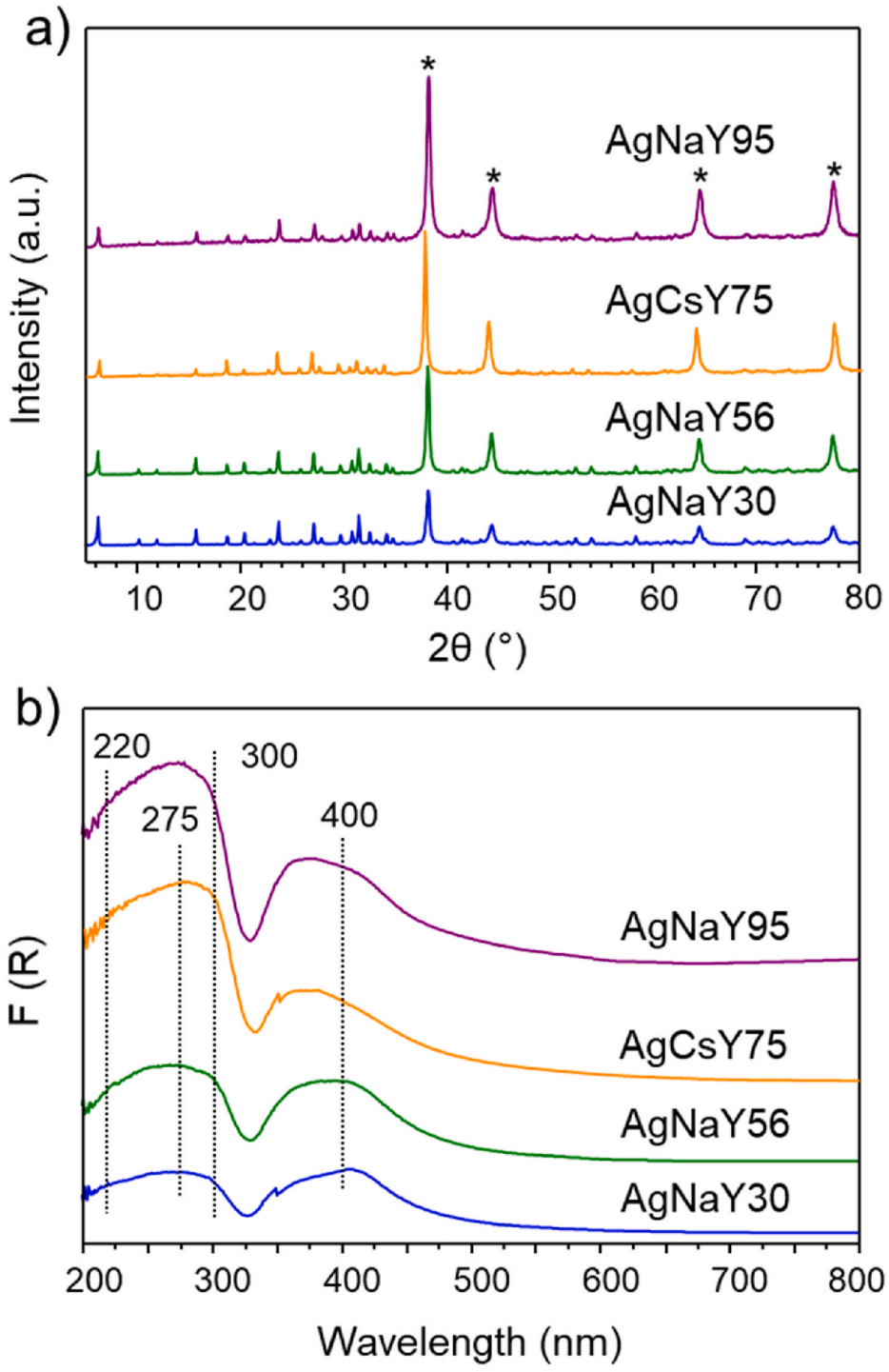

Fig. 3. X-ray diffraction patterns (a) and UV–Vis spectra (b) of AgNaY30, AgNaY56, AgCsY75 and AgNaY95 zeolites. (* diffraction peaks of Ag^0 metal).

Debye-Waller (D-W) factor (σ^2) and amplitude has been minimized adopting a co-refinement approach leaving only one Debye-Waller factor for the same dataset. Fitting individual Debye-Waller factors resulted in similar values for N_{Ag-Ag} but higher error bars. Meanwhile, considering a common D-W factor (0.0103 $Å^2$) i.e., assuming that all samples have the same static disorder, give good quality fits and correlation factor below 0.7 for all Ag-zeolites. Although the N_{Ag-Ag} and R_{Ag-Ag} point out to the formation of bulk silver, that is, particle sizes larger than about 5 nm [57], the D-W factor is slightly higher than that of the metal reference indicating higher static disorder, often observed for similar systems based on noble metal NPs [58].

The observation of metal particles smaller than 10 nm by TEM and of $[Ag_m]^{\delta+}$ and $[Ag_n]^0$ clusters by UV–Vis in the AgNaY95 zeolite could appear to be in contradiction with the EXAFS results. However, since XAS is a bulk technique, the signal is dominated by metal Ag particles covering the signal coming from existing nanoclusters, which has been demonstrated in the literature [57].

Fig. 6a and b shows the activity and selectivity to N_2 of Ag-zeolites in the NH_3–SCO reaction as a function of the temperature. The results of Fig. 6a indicates that the NH_3 conversion increases with the silver loading, reaching almost 100% at 300 °C for AgNaY95 and AgCsY75 zeolites. Assuming that silver particles are the active sites for the

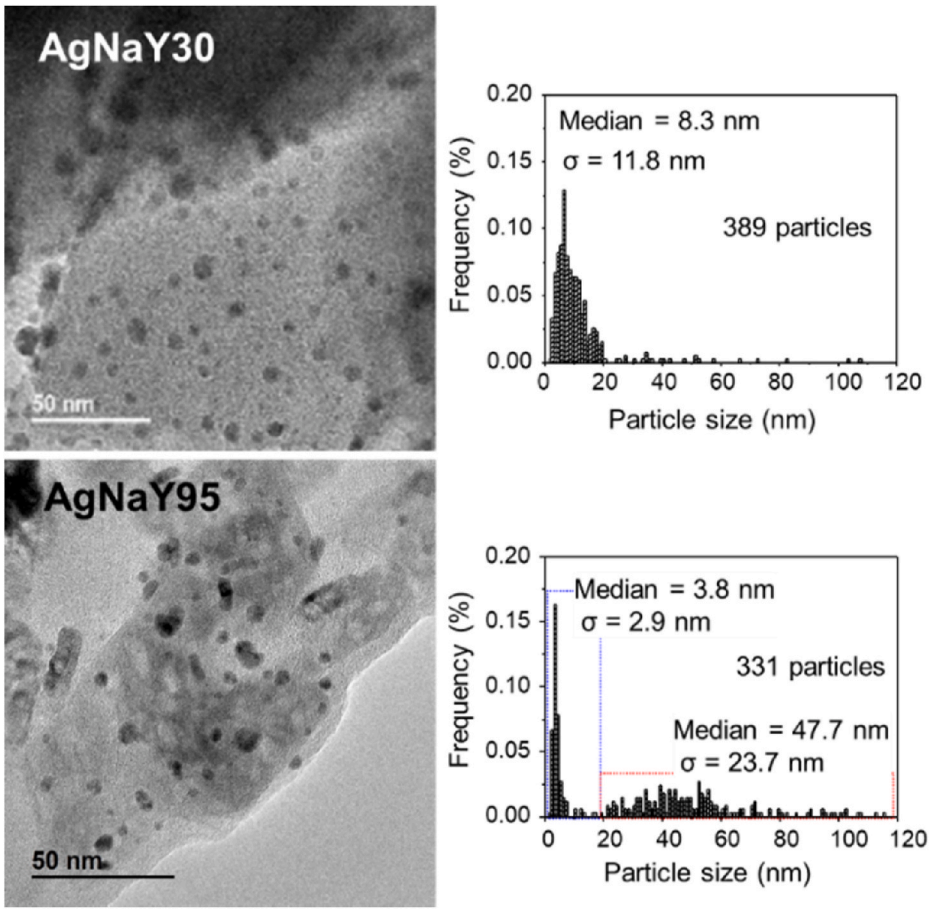

Fig. 4. TEM images (left) and particle size distribution (right) of AgNaY95 and AgNaY30 zeolites.

reaction, this result indicates that zeolite AgNaY95 with the higher silver content has more surface metal sites active for the reaction in spite of the smaller metal dispersion. The activity per surface silver atom was roughly estimated at 20% NH_3 conversion considering the NPs size using the method described previously [13,14]. Similar TOF values were calculated for AgNaY95 and AgNaY30 zeolites (4.9 and 4.1 s^{-1}, respectively), suggesting that the intrinsic activity of surface silver sites does not greatly depend on the particle size. This is further supported by the linear decrease of the $T_{50\%}$ (the temperature for 50% ammonia conversion) of the AgNaY zeolites with the silver content (represented in Fig. 6c). Fig. 6b shows that the selectivity to N_2 in the NH_3-SCO reaction increases with the temperature for all Ag-zeolites, being accompanied mainly by N_2O and less than 5% of NO in the temperature range 350 °C–400 °C. Considering AgNaY zeolites, the selectivity to N_2 decreases with the silver content as follows: AgNaY95 > AgNaY56 > AgNaY30. The activity and selectivity on AgCsY75 are only slightly lower than those on AgNaY95.

The catalyst stability during the NH_3–SCO reaction was tested on the more active AgNaY95 zeolite at 300 °C (95% ammonia conversion) with a used catalyst, showing a decrease of about 5% after 16 h of catalytic reaction time. The selectivity to N_2 was kept at 60% indicating that the catalytic performance is very stable.

3.1.1. *Influence of the compensating cation on the AgY based catalysts for the NH_3–SCO reaction*

In the as prepared AgY zeolites the negative charges from the framework are compensated by Ag^+ and the alkaline cation (Na^+ or Cs^+). Upon the treatment under hydrogen, Ag^+ is reduced to Ag^0 or positively charged clusters, generating Brønsted acid sites while the alkaline cation act as compensating cation stabilizing the zeolite structure. In order to check if the use of Na^+ or Cs^+ may affect the characteristic and performance of AgY based catalysts, the AgCsY75 zeolite containing Cs^+ instead of Na^+ was studied (see chemical composition in Table 1). The XRD patterns and the UV–Vis spectra of the AgCsY75 zeolite are included in Fig. 3 and the catalytic results in Fig. 6. The X-ray diffractogram indicates the presence of metal particles and the UV–Vis spectrum show that, as the AgNaY, the AgCsY75 zeolite also contains positively charged and neutral clusters as well as metal NPs. The shape of the UV–Vis spectrum of the AgCsY75 zeolite, with an intermediate silver content between AgNaY56 and AgNaY95, is closer to the latter suggesting that the relative content of the different species are closer to the AgNaY with higher silver loading. This is supported by the catalytic activity for the NH_3-SCO reaction shown in Fig. 6, since the AgCsY75 gives a 50% NH_3 conversion at T_{50} = 210 °C, much closer to AgNaY95 (T_{50} = 200 °C) than to AgNaY56 (T_{50} = 250 °C). The same accounts for the selectivity to N_2 of the AgCsY75 catalyst, as it follows a similar trend than that of the AgNaY95 sample. These results point out that the larger size of Cs^+ favour the formation of metal NPs, which are the actual active sites for the NH_3–SCO reaction, on the outer surface of the AgCsY zeolite, giving somewhat higher activity than the analogous AgNaY zeolite. As the general features are similar for AgCsY and AgNaY zeolites, a more detailed study is focused on the AgNaY catalysts.

3.2. *Transformation of silver species in AgNaY zeolites during the NH_3–SCO reaction*

The silver species are sensitive to the gases used for thermal treatments [14,36,37] and then, it may be of interest the characterization of the AgNaY zeolites after the catalytic testing at 400 °C in order to assess the changes that may experience the Ag species during the NH_3–SCO

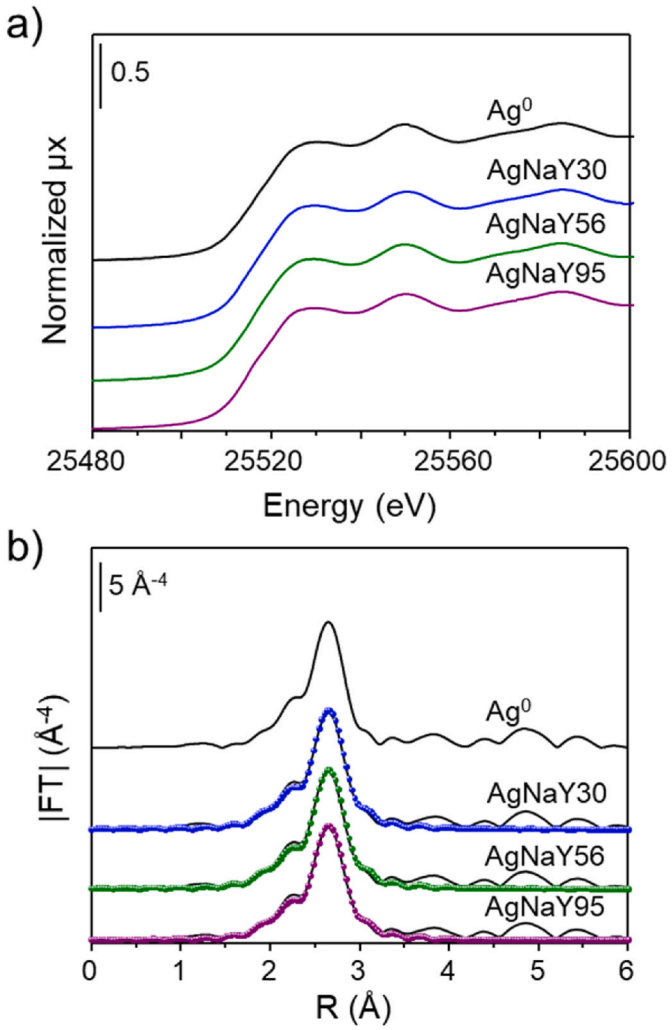

Fig. 5. Normalized XANES spectra (a) and |FT| of the k^3-weighted χ(k) functions (black line: experimental, color points: simulation) (b) of Ag-containing catalysts after reduction in H_2. (For interpretation of the references to color in this figure legend, the reader is referred to the Web version of this article.)

Table 2
Summary of optimized parameters by fitting EXAFS data of catalysts after reduction in H_2[a].

Sample	$N_{Ag\text{-}Ag}$	$R_{Ag\text{-}Ag}$ (Å)	σ^2 (Å^2)	ΔE_0 (eV)	R_{factor}
Ag metal	12	2.863 ± 0.006	0.0097 ± 0.0003	2.7 ± 0.3	0.0018
AgNaY30	12.0 ± 0.3	2.859 ± 0.002	0.0103 ± 0.0001	2.7 ± 0.1	0.0034
AgNaY56	12.0 ± 0.2	2.861 ± 0.001			0.0024
AgNaY95	11.7 ± 0.3	2.860 ± 0.002			0.0025

[a] The fits were performed on the first coordination shell (ΔR = 2.0–3.0 Å) over FT of the k^3-weighted χ(k) functions performed in the Δk = 2.3–14.0 Å^{-1} interval, resulting into a number of independent parameters of $2\Delta R\Delta k/\pi = 28.2$ (7 for Ag metal). Non-optimized parameters are recognizable by the absence of the corresponding error. $S_0^2 = 0.81$ from Ag metal.

reaction.

The XRD patterns of the used AgNaY zeolites show only a decrease in the intensities of the characteristic X-ray diffraction peaks of metallic silver (not shown) suggesting a diminution in the number of metallic NPs. The modification of the silver species present in the AgNaY zeolites

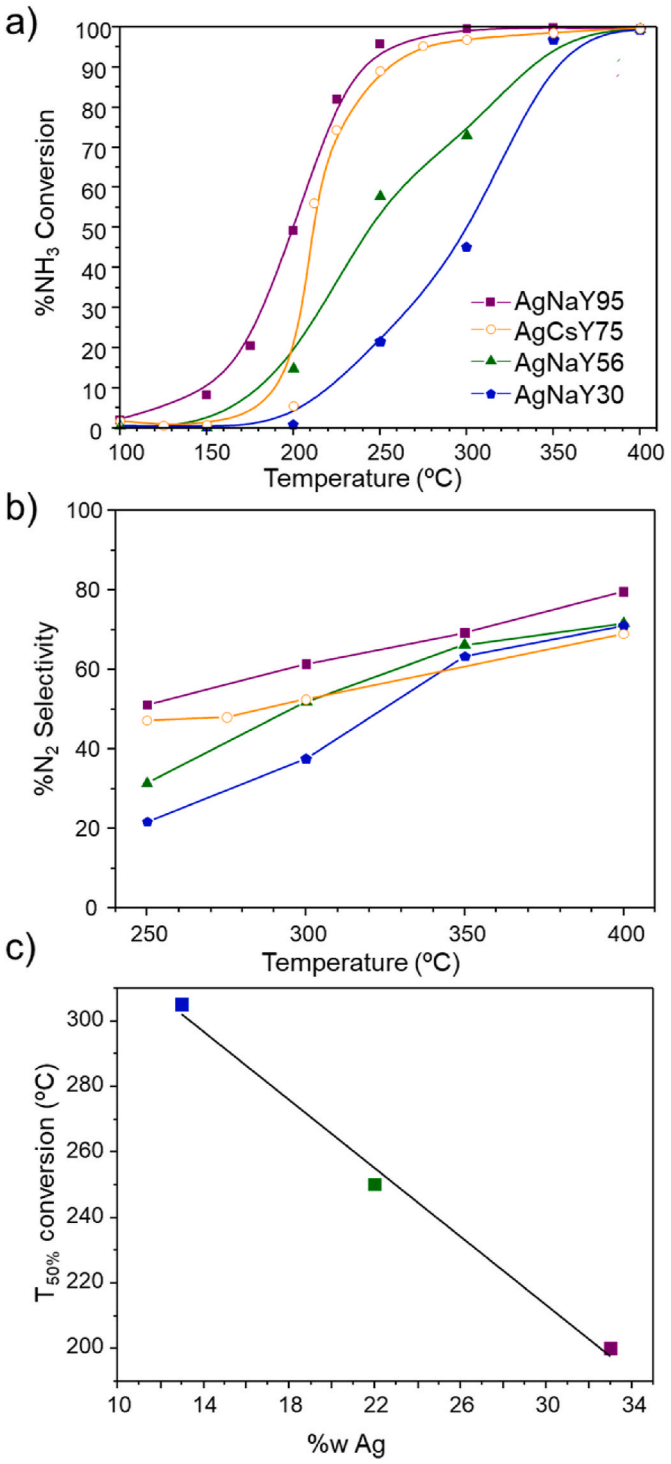

Fig. 6. The results of the NH_3–SCO reaction on AgNaY and AgCsY75 zeolites: a) NH_3 conversion and b) N_2 selectivity as a function of the temperature. c) $T_{50\%}$ (Temperature of 50% conversion) as a function of the silver loading in the catalysts on the NH_3–SCO.

was confirmed by UV–Vis spectroscopy as shown in Fig. 7a (compare with Fig. 3). After the catalytic tests, all AgNaY zeolites show an UV band at 220 nm assigned to atomically dispersed Ag^+. This band is accompanied by other absorption bands at 275 nm and 300 nm attributed to the presence of $[Ag_m]^{\delta+}$ and $[Ag_n]^0$ clusters respectively, and a very broad component at 430 nm of Ag^0 assigned to metallic NPs [30, 51]. The relative intensities of these bands change in the different samples, indicating that the proportion of these species varies with the

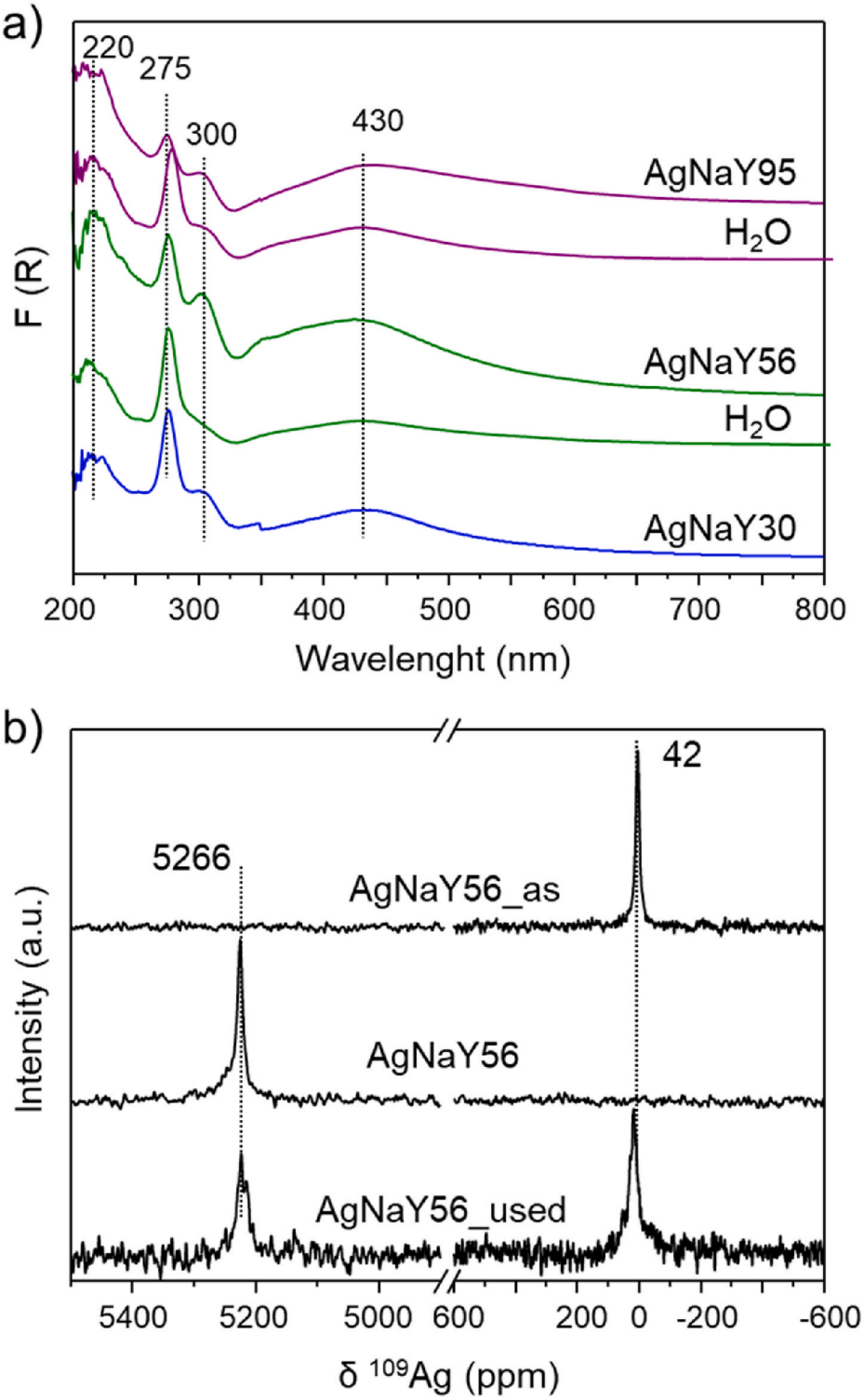

Fig. 7. a) UV–Vis spectra of the used AgNaY catalysts b) ^{109}Ag Solid-State NMR spectra of the AgNaY56 catalyst as prepared (AgNaY56_as), reduced under hydrogen (AgNaY56) and after the NH_3–SCO reaction (AgNaY56_used).

Ag content of the AgNaY zeolites. As an overall conclusion from the UV–Vis spectra, it can be said that the metallic NPs and Ag clusters species present in the reduced Ag-zeolite catalysts are re-dispersed and oxidized to isolated Ag^+ species during the NH_3–SCO reaction. This is further supported by ^{109}Ag MAS NMR spectroscopy as illustrated in Fig. 7b for the AgNaY56 zeolite. The spectrum of the as-prepared zeolite (AgNaY56_as) consists of a unique peak at δ ^{109}Ag ≈ 42 ppm assigned to Ag^+, whilst the reduced catalyst (AgNaY56) gives a peak at δ ^{109}Ag ≈ 5570 ppm attributed to Ag^0 [39,59]. The spectrum of the used zeolite shows the contribution of both Ag^0 and Ag^+ species, confirming that silver has been oxidized to Ag^+ during the reaction. The quantitative analysis of the spectrum indicates that approximately 60% of total silver appears as cationic Ag^+ species in the Ag-zeolite catalyst used.

Fig. 8 shows the TEM and the PSD of AgNaY30 and AgNaY95 zeolites after reaction. Comparison with Fig. 4 shows that the particle size distribution of the used AgNaY30 zeolite is very similar to that of the

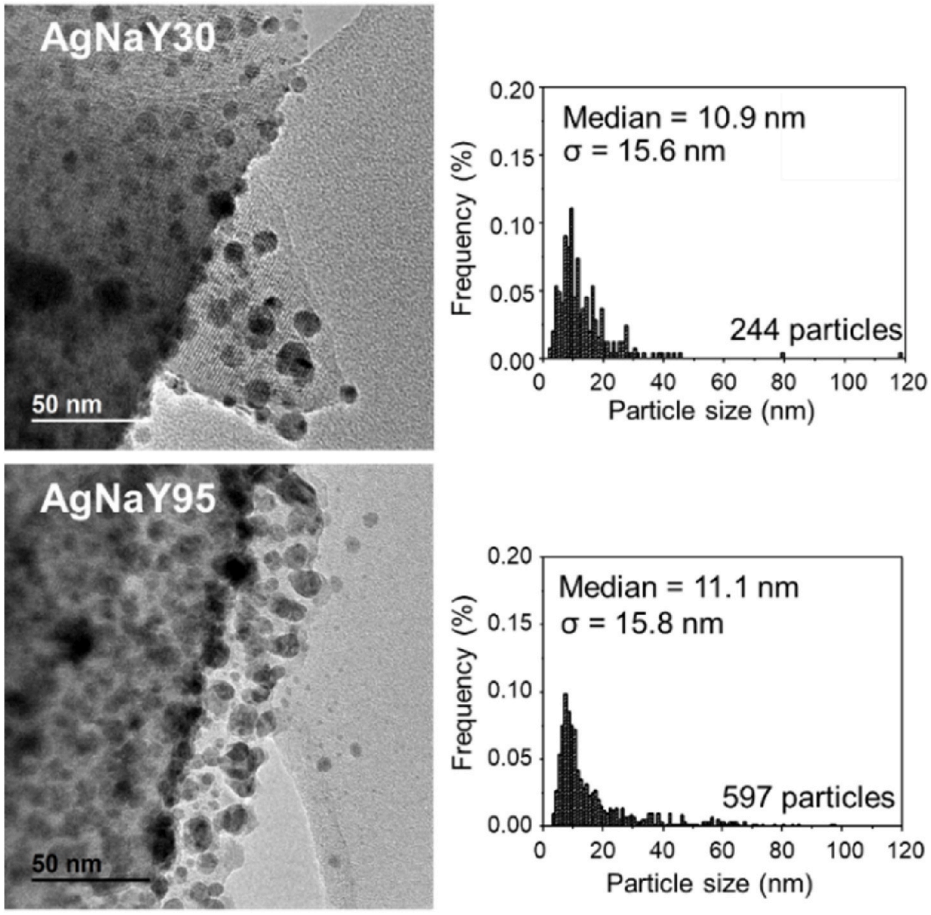

Fig. 8. Representative TEM images (left) and particle size distribution (right) of AgNaY95, AgNaY30 zeolites after the catalytic test.

reduced sample. However, the PSD of the AgNaY95 is strongly modified during the course of the NH_3–SCO-reaction. Indeed, the bimodal distribution of the reduced AgNaY95 zeolite (Fig. 4) practically disappears after reaction (Fig. 8). The very small Ag particles of sizes around 4 nm in the original sample becomes broader and slightly larger, but significantly, the big particles of >20 nm practically disappear in the used catalyst. Thus, after reaction, the PSD of both used AgNaY catalysts have very similar profiles regardless of the Ag loading of the catalyst.

The changes in the state of aggregation of silver in the AgNaY95 and AgNaY30 zeolites during the NH_3–SCO reaction was investigated by *in situ* XAS spectroscopy recording the spectra in the presence of the reactant mixture at 300 °C and 550 °C and then, after cooling down to room temperature under He to increase data quality minimizing thermal vibrations. As can be observed in Fig. 9, the XANES spectra and the |FT| of the EXAFS signals of the AgNaY95 and AgNaY30 zeolites are very different from the reduced catalysts where metal is dominant (Fig. 5). The |FT| of the Ag-zeolites show two peaks at ca. 1.6 Å and 2.6 Å (without phase correction) of Ag–O pair from cationic Ag species and of Ag–Ag from clusters and metallic silver respectively. The peak of the Ag–Ag pair is weak when compared with the metal (see the multiplication factor), asymmetric because of the overlapping with higher shells of cationic species and neutral clusters of silver and the shape (see split in the |FT| of Fig. 9b) changes with the temperature. The slight decrease in the peak intensity by heating from 300 °C to 500 °C is due to thermal disorder, as proved by the intensity recovery observed at room temperature.

The combination of thermal effects and the overlapping between Ag^0, Ag clusters and Ag^+ signals make a quantitative estimation of N_{Ag-Ag} during and after reaction conditions very difficult and not reliable. Anyhow, the results reported here indicate that silver particles are certainly re-dispersed and re-oxidized to atomically dispersed Ag^+ species during the NH_3–SCO reaction.

Finally, to check the reversibility of the changes suffered by the silver clusters and particles, the AgNaY95 zeolite used in the reaction was again reduced under H_2 at 400 °C, named as _REG, as shown in Fig. 10, the catalyst recovers the intensity of the X-ray diffraction peaks of Ag^0 and the profile of the UV–Vis spectrum reveals the agglomeration of silver atoms.

3.3. *The influence of water in the catalytic performance of AgNaY zeolites in NH_3–SCO reaction*

The catalytic performance of the AgNaY95 and AgNaY56 zeolites in the NH_3–SCO reaction has been tested in the presence of water in the reaction feed in order to simulate a real exhaust conditions. The results are shown in Fig. 11a which also includes the catalytic test without water for comparison purposes. As can be observed, the catalyst activity only slightly decreases under humid conditions, so that T_{50} shifts about 70 °C to higher temperature for the AgNaY95 (to $T_{50} \approx 275$ °C) and only about 25 °C (to $T_{50} \approx 275$ °C) for the AgNaY56 zeolite. Also small modifications are observed for the selectivity to N_2 (Fig. 11b). The changes in the catalytic behaviour are in the range of those previously reported for other silver-based catalyst, indicating that AgNaY zeolites are relatively stable catalysts for the NH_3–SCO reaction in the presence of water [13,36,41].

The UV–Vis spectra of the AgNaY95 and AgNaY56 zeolites recorded after the reaction in the presence of water are included in Fig. 7. All the spectra contain the same bands than those recorded after the reaction in the absence of water, indicating the occurrence of similar silver species: Ag^+ (220 nm), $[Ag_m]^{\delta+}$ (275 nm), $[Ag_n]^0$ (300 nm) and metallic Ag^0 NPs

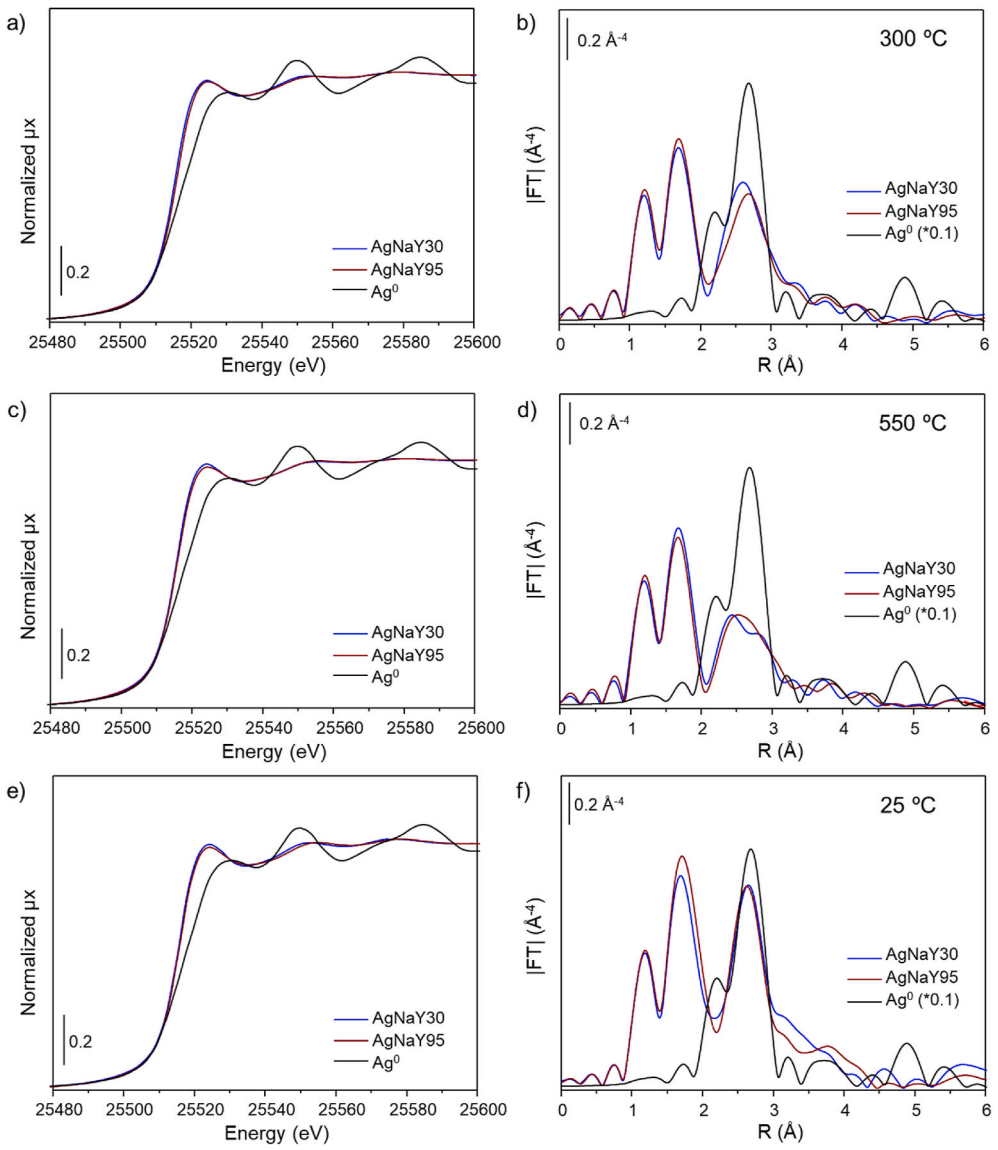

Fig. 9. Normalized XANES spectra (left) and |FT| of the k^3-weighted χ(k) functions (right) of AgNaY zeolites-containing NH_3–O_2 mixture recorded at a-b) 300 °C, c-d) 550 °C, e-f) 25 °C. The |FT| of metallic silver was divided by 10 for better visualization of the results.

(400 nm), while the different shape indicates that they are in different concentration. The results reported in Fig. 7 indicate that the addition of water into the reaction feed decreases the amount of metal NPs and increases the formation of cationic silver species during the catalytic test.

4. Discussion

The results reported here indicate that isolated Ag^+ species in as-prepared AgNaY zeolites are not reduced upon the treatment under O_2 or N_2. Inspection of the data reported in the bibliography points out that the reducibility of Ag^+ strongly depends on the zeolite structure and chemical composition such as the Si/Al ratio or the presence of Brønsted acid sites [29,36,39,50,51]. In the case of this study, it can be concluded that aluminum-rich AgNaY zeolites, with high silver loading ranging between 10 wt % and 30 wt % and not possessing acidic protons, require a treatment under H_2 to sensitively reduce Ag^+ resulting in the formation of $[Ag_m]^{\delta+}$ and $[Ag_n]^0$ clusters and metallic NPs, being their particle size distribution highly dependent on the Ag loading.

Our results demonstrate that atomically dispersed Ag^+ (with or without the presence of Brønsted acid sites) are essentially non-active for the NH_3–SCO reaction and indeed, the catalytic activity of AgNaY zeolite before reduction, which contains exclusively Ag^+, is similar to that found for the thermal reaction without any catalyst. However, the Ag-containing zeolite catalysts develop a noticeable catalytic activity for the NH_3–SCO reaction when they are reduced under H_2, giving rise to the formation of metallic silver.

In the most active AgNaY95 zeolite, the metallic Ag^0 NPs are partially blocking the pores aperture diminishing the diffusion of gas molecules within the zeolite channels and cavities where most clusters must be placed. This supports the idea that Ag^0 NPs are the active sites for the reaction or at least are the precursors of the Ag active species for the first step in NH_3-SCO reaction. In spite of having larger metal particles, the higher activity of the AgNaY95 catalyst is due to its higher metal loading and to a larger number of surface metal active sites accessible for the reaction. The selectivity to N_2 on AgNaY catalysts is increased at high reaction temperature (300–400 °C) and with the silver content, supporting that the N_2 selectivity is enhanced on large metal particles [10,11,26]. For the most active AgNaY95 zeolite, 100% ammonia conversion is reached at 300 °C (T_{100} = 300 °C) with a N_2 selectivity of about 60%, whereas the less active AgNaY30 requires a temperature of 400 °C for total conversion with a N_2 selectivity of 70%.

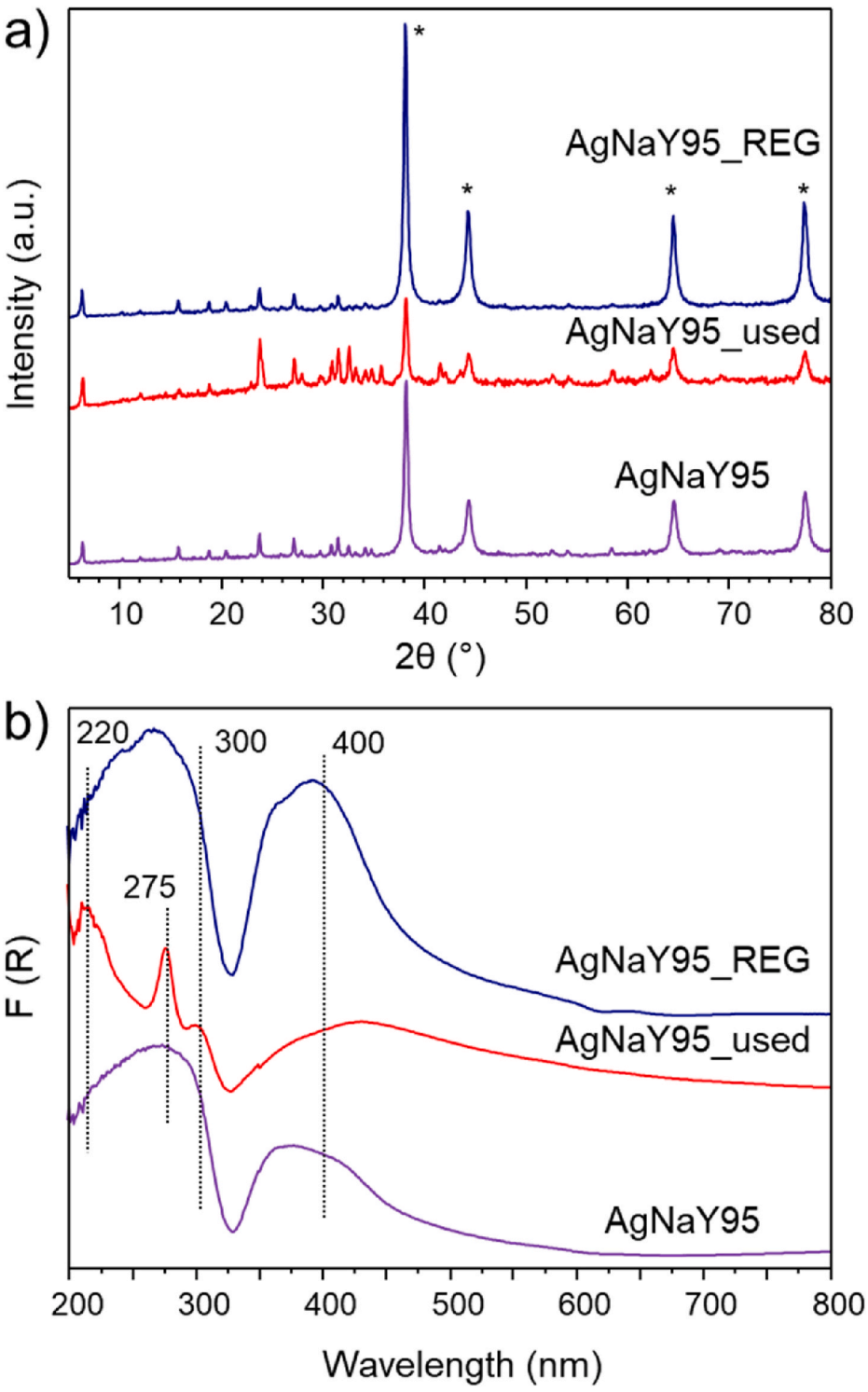

Fig. 10. (a) X-ray diffractograms and (b) UV–Vis spectra of the AgNaY95 zeolite, from bottom to top: reduced under H_2 flow at 400 °C (AgNaY95), after the catalytic test (AgNaY95_used) and subsequently treated under H_2 flow at 400 °C (AgNaY95_REG).

Considering the N_2 selectivity, this is within the range 71%–79% at 400 °C and 61%–69% at 350 °C for all AgNaY catalysts, being only for the AgNaY95 sample relatively high ~60% when lowering the temperature at 300 °C. Therefore, high silver loading on AgNaY zeolites improves the catalytic conversion of ammonia and the selectivity to N_2, being especially relevant at 300 °C or lower temperatures [16,37]. The presence of bulkier Cs^+ instead of Na^+ as compensating cation favours the formation of metal NPs, slightly increasing the activity for the NH_3–SCO reaction. It must be noted that the most active AgNaY95 catalyst maintains its activity for 16 h of continuous reaction.

Characterization of the used catalyst evidences deep changes in the speciation of silver in the AgNaY zeolites during the NH_3–SCO reaction. Silver metal particles are re-dispersed to give neutral or positively charged Ag clusters and even oxidized to monoatomic Ag^+ cations. The presence of these Ag^+ has been fully proved employing UV–Vis and ^{109}Ag NMR spectroscopies, and the latter shows that about 60% of silver

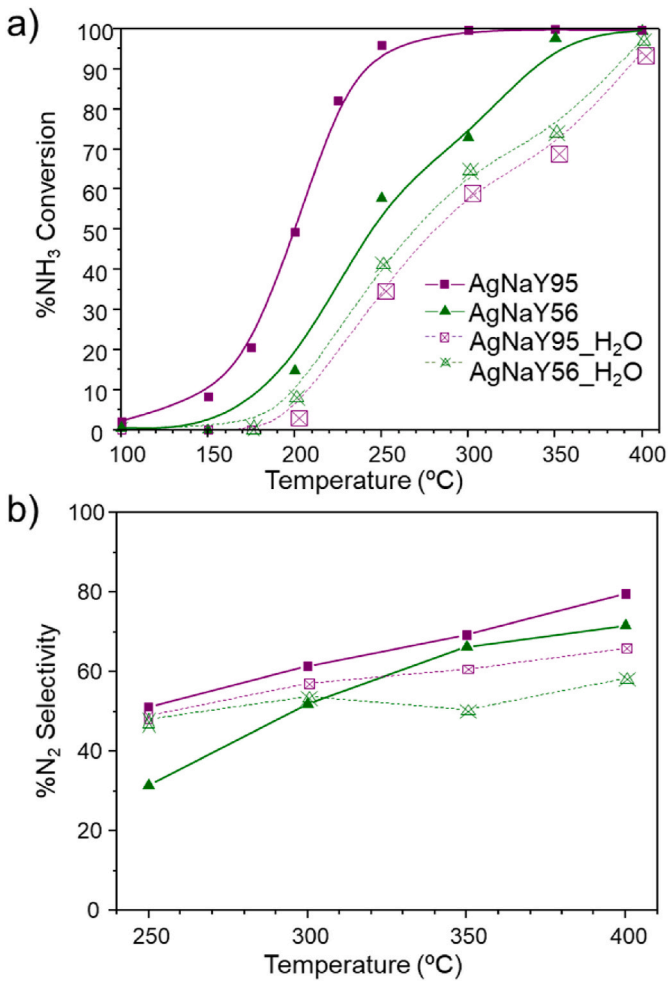

Fig. 11. Results of the NH_3–SCO reaction on AgNaY56 and AgNaY95 zeolites including 3% of water vapour: a) NH_3 conversion and b) N_2 selectivity as a function of the temperature.

is in the form of Ag^+ in the used AgNaY56 zeolite catalyst. Meanwhile, EXAFS results show that the average particle size has largely decreased according to the intensity decrease of Ag–Ag contribution, being consistent with particle size distribution calculated from TEM images. Therefore, it comes out that although some silver particles remain, most have been dispersed forming neutral and charged clusters and more than half Ag atoms are oxidized to dispersed Ag^+.

The most accepted mechanism for the NH_3–SCO reaction, especially for temperatures above 200 °C is the i-SCR which occurs on two steps, first the NH_3 is oxidized to NO and then the NO is reduced with non-reacted NH_3 to give N_2 and H_2O (NH_3-SCR-NO), as shown in equations (1) and (2). However, ammonia can also be oxidized to N_2O, which is the main by-product in the reaction within the temperature range studied here, according to equation (3).

$$4\ NH_3 + 5\ O_2 \rightarrow 4\ NO + 6\ H_2O \quad (1)$$

$$4\ NO + 4\ NH_3 + O_2 \rightarrow 4\ N_2 + 6\ H_2O \quad (2)$$

$$2\ NH_3 + 2\ O_2 \rightarrow N_2O + 3\ H_2O \quad (3)$$

The Ag speciation observed for the AgNaY catalysts is fully consistent with previous publications on the NH_3–SCO reaction pathways on Ag-based catalysts which is shown in Scheme 1:

During the activation step of the AgY catalyst by heating under H_2, the compensating Ag^+ cations are reduced to metallic Ag NPs resulting in the formation of Brønsted acid sites (H^+) for charge compensation. The formation of metallic silver NPs is fully probed by X-ray diffraction, ^{109}Ag MAS-NMR, TEM and XAS spectroscopy as previously discussed.

The NH_3–SCO-reaction may be split into two consecutive steps: i) The first one consists on the catalytic oxidation of NH_3 by oxygen giving rise to the formation of adsorbed nitrate anions, which have been previously observed on silver-based catalysts [14,36], and positively charged Ag species. Nitrates are stable reaction intermediates which are assumed to be formed by oxidation of NO coming from the oxidation of NH_3. Our results prove that the presence of metallic Ag^0 is mandatory for achieving nitrate formation since non-activated AgFAU catalysts were inactive and XAS and UV–Vis spectroscopies indicate that no Ag^+ reduction occurs by heating the Ag^+-exchanged faujasite catalyst precursor under an inert atmosphere. This strongly supports that Ag^0 are the active sites for the first ammonia oxidation step, while Ag^+ is catalytically inactive for this first reaction step. Ammonia oxidation can also form N_2O especially at low reaction temperatures that is released to the product gas stream. The absence of NO in the reaction products suggests that NO readily evolves to nitrate species, which has been proposed as the initial step of an i-SCR mechanism of the NH_3–SCO reaction on Ag-alumina and AgY zeolite catalysts [14,36] resulting in the oxidation of Ag^0 to Ag^+ species. ii) In the second step, adsorbed nitrate and ammonium ions are selectively transformed to molecular nitrogen and water on the cationic Ag^+ sites, which are reduced to metallic Ag, being ready for starting a new catalytic cycle.

This mechanism is fully consistent with our results. Indeed, *in situ* XAS experiments show that Ag^+ and metallic Ag^0 species are present in the catalysts during the NH_3–SCO reaction as discussed before. Also, Ag^+ and Ag^0 have been clearly identified in the used-AgNaY catalysts by UV–Vis and ^{109}Ag-NMR techniques. Then, both Ag species must coexist in the active catalyst during the course of the NH_3–SCO process.

The results obtained with water in the reaction feed leads to the conclusion that humidity favours the re-dispersion and oxidation of the silver metal NPs that are the actual active sites for the initial oxidation of NH_3 to NO, and accordingly the activity and selectivity of the AgNaY catalyst decrease. Nevertheless, the changes observed in the catalytic performance of the AgNaY catalysts prove that they are relatively stable, comparable to other silver based catalysts reported in the bibliography [13,36].

Therefore, the redox properties of silver-based catalysts, which depend on the loading and the characteristic of the support, must be

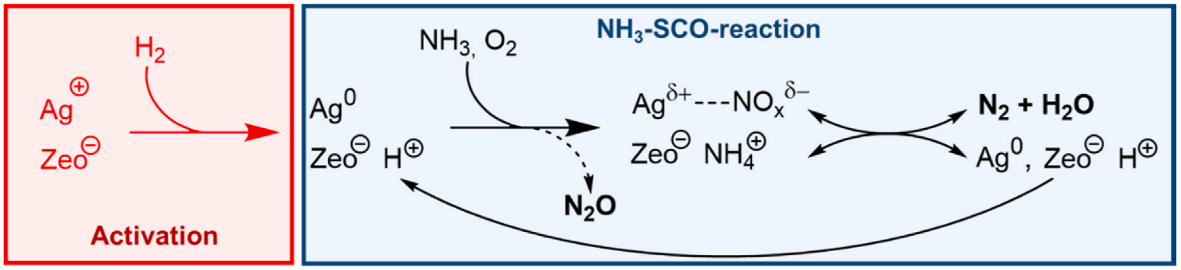

Scheme 1. NH_3–SCO reaction pathway using Ag-Zeolites.

very relevant for the NH_3-SCO reaction. For Ag-zeolites, the redox behaviour of silver will be determined by the framework topology, the Si/Al molar ratio and the presence of Brønsted and Lewis acid sites. All these parameters should be optimized for developing a catalyst active and selective for the NH_3–SCO process [60]. Although this reaction has been investigated on Ag/Al_2O_3 catalysts, there are only very few studies on Ag-zeolites and then there is still a place for further research.

5. Conclusions

To summarize, our results on the NH_3–SCO reaction over AgNaY catalysts with silver contents in the range (Ag/Al = 0.30–0.95) indicate that the zeolites must be reduced with H_2 to form Ag^0, which are the active centres for the reaction. Ag^+, which is the only silver species present in the AgY zeolites as-prepared or after being activated in the presence of O_2 or N_2 are inactive for the ammonia oxidation. The reduced catalysts contain mainly neutral and/or charged clusters and metal NPs with an average size that increases with the silver content. The catalyst activity and the selectivity to N_2 increase also with the silver loading. The AgNaY zeolites are dramatically modified during the NH_3–SCO reaction being metal particles dispersed so that more than half silver is in the form of atomically dispersed Ag^+. Assuming the i-SCR mechanism, the ammonia would be first oxidized to NO_3^- on the metal particles, accompanied by partial oxidation of silver. The NO_3^- would then react with ammonia to be reduced to N_2 and water, which should be accompanied by the reduction to Ag^0 ready to start a new catalytic cycle. Several silver species with different oxidation states, Ag^0 NPs, and Ag^+, besides $[Ag_m]^{\delta+}$ or $[Ag_n]^0$ are present during the NH_3–SCO reaction on Ag-zeolites. The addition of water in the feed promotes the dispersion of metallic silver and the appearance of cationic silver species, slightly decreasing the catalyst activity and selectivity. Nevertheless, the AgNaY zeolites are relatively stable under reaction condition. In this way, the redox properties of the silver species, which depend on the loading and the characteristic of the zeolite support, take a great relevance on the NH_3-SCO reaction.

CRediT authorship contribution statement

Joaquin Martinez-Ortigosa: Investigation, Writing – original draft. **Christian W. Lopes:** Investigation, Writing – original draft. **Giovanni Agostini:** Investigation, Writing – original draft. **A. Eduardo Palomares:** Investigation. **Teresa Blasco:** Methodology, Conceptualization, Writing – review & editing. **Fernando Rey:** Supervision, Project administration, Writing – review & editing.

Declaration of competing interest

The authors declare that they have no known competing financial interests or personal relationships that could have appeared to influence the work reported in this paper.

Acknowledgments

Financial support by the Ministerio de Ciencia e Innovación (MICINN) of Spain through the Severo Ochoa (SEV-2016-0683), RTI2018-101784-B-I00, RTI2018-09639-A-I00 and InnovaXN-26-2019 projects is gratefully acknowledged. The authors also thank the Microscopy Service of the Universitat Politècnica de València for its assistance in microscopy characterization (TEM and FESEM equipment preparation). C. W. Lopes (Science without Borders - Process no. 13191/13–6) thanks CAPES for a predoctoral fellowship and J. Martínez-Ortigosa (SEV-2012-0267-02) is grateful to Severo Ochoa Program for a predoctoral fellowship. The authors also want to thank the ALBA synchrotron and CLÆSS beamline staff for providing beam-time (proposal 2017092477) and for setting the beamline up to perform these studies.

References

[1] R. Zhang, N. Liu, Z. Lei, B. Chen, Selective transformation of various nitrogen-containing exhaust gases toward N2 over zeolite catalysts, Chem. Rev. 116 (2016) 3658–3721.
[2] L. Chmielarz, M. Jabłońska, Advances in selective catalytic oxidation of ammonia to dinitrogen: a review, RSC Adv. 5 (2015) 43408–43431.
[3] C.K. Lambert, Perspective on SCR NOx control for diesel vehicles, Reaction Chem. Eng. 4 (2019) 969–974.
[4] L. Han, S. Cai, M. Gao, J.-y. Hasegawa, P. Wang, J. Zhang, L. Shi, D. Zhang, Selective catalytic reduction of NOx with NH3 by using novel catalysts: state of the art and future prospects, Chem. Rev. 119 (2019) 10916–10976.
[5] R.S. Ghosh, T.T. Le, T. Terlier, J.D. Rimer, M.P. Harold, D. Wang, Enhanced selective oxidation of ammonia in a Pt/Al2O3@Cu/ZSM-5 core–shell catalyst, ACS Catal. 10 (2020) 3604–3617.
[6] E.K. Dann, E.K. Gibson, R.H. Blackmore, C.R.A. Catlow, P. Collier, A. Chutia, T. E. Erden, C. Hardacre, A. Kroner, M. Nachtegaal, A. Raj, S.M. Rogers, S.F.R. Taylor, P. Thompson, G.F. Tierney, C.D. Zeinalipour-Yazdi, A. Goguet, P.P. Wells, Structural selectivity of supported Pd nanoparticles for catalytic NH3 oxidation resolved using combined operando spectroscopy, Nat. Catal. 2 (2019) 157–163.
[7] T. Lan, Y. Zhao, J. Deng, J. Zhang, L. Shi, D. Zhang, Selective catalytic oxidation of NH 3 over noble metal-based catalysts: state of the art and future prospects, Catal. Sci. Technol. 10 (2020) 5792–5810.
[8] S. Hinokuma, S. Kiritoshi, Y. Kawabata, K. Araki, S. Matsuki, T. Sato, M. Machida, Catalytic ammonia combustion properties and operando characterization of copper oxides supported on aluminum silicates and silicon oxides, J. Catal. 361 (2018) 267–277.
[9] A.C. Akah, G. Nkeng, A.A. Garforth, The role of Al and strong acidity in the selective catalytic oxidation of NH3 over Fe-ZSM-5, Appl. Catal. B Environ. 74 (2007) 34–39.
[10] M. Jabłońska, R. Palkovits, Copper based catalysts for the selective ammonia oxidation into nitrogen and water vapour—recent trends and open challenges, Appl. Catal. B Environ. 181 (2016) 332–351.
[11] F. Gao, Y. Liu, Z. Sani, X. Tang, H. Yi, S. Zhao, Q. Yu, Y. Zhou, Advances in selective catalytic oxidation of ammonia (NH3–SCO) to dinitrogen in excess oxygen: a review on typical catalysts, catalytic performances and reaction mechanisms, J. Environ. Chem. Eng. (2020) 104575.
[12] Z. Liu, J. Zhu, J. Li, L. Ma, S.I. Woo, Novel Mn–Ce–Ti mixed-oxide catalyst for the selective catalytic reduction of NOx with NH3, ACS Appl. Mater. Interfaces 6 (2014) 14500–14508.
[13] F. Wang, J. Ma, G. He, M. Chen, C. Zhang, H. He, Nanosize effect of Al2O3 in Ag/Al2O3 catalyst for the selective catalytic oxidation of ammonia, ACS Catal. 8 (2018) 2670–2682.
[14] F. Wang, G. He, B. Zhang, M. Chen, X. Chen, C. Zhang, H. He, Insights into the activation effect of H2 pretreatment on Ag/Al2O3 catalyst for the selective oxidation of ammonia, ACS Catal. 9 (2019) 1437–1445.
[15] L. Gang, B.G. Anderson, J. van Grondelle, R.A. van Santen, Low temperature selective oxidation of ammonia to nitrogen on silver-based catalysts, Appl. Catal. B Environ. 40 (2003) 101–110.
[16] L. Zhang, C. Zhang, H. He, The role of silver species on Ag/Al2O3 catalysts for the selective catalytic oxidation of ammonia to nitrogen, J. Catal. 261 (2009) 101–109.
[17] M. Zhou, Z. Wang, Q. Sun, J. Wang, C. Zhang, D. Chen, X. Li, High-performance Ag–Cu nanoalloy catalyst for the selective catalytic oxidation of ammonia, ACS Appl. Mater. Interfaces 11 (2019) 46875–46885.
[18] H. Deng, Y. Yu, H. He, Water effect on preparation of Ag/Al2O3 catalyst for reduction of NOx by ethanol, J. Phys. Chem. C 120 (2016) 24294–24301.
[19] P.I. Kyriienko, Selective catalytic reduction of NOx with ethanol and other C1–4 oxygenates over Ag/Al2O3 catalysts: a review, Front. Chem. Sci. Eng. 14 (2019) 471–491.
[20] J.P. Breen, R. Burch, A review of the effect of the addition of hydrogen in the selective catalytic reduction of NOxwith hydrocarbons on silver catalysts, Top. Catal. 39 (2006) 53–58.
[21] N. Serhan, A. Tsolakis, A. Wahbi, F. Martos, S. Golunski, Modifying catalytically the soot morphology and nanostructure in diesel exhaust: influence of silver De-NOx catalyst (Ag/Al2O3), Appl. Catal. B Environ. 241 (2019) 471–482.
[22] G. Xu, J. Ma, L. Wang, W. Xie, J. Liu, Y. Yu, H. He, Insight into the origin of sulfur tolerance of Ag/Al2O3 in the H2-C3H6-SCR of NOx, Appl. Catal. B Environ. 244 (2019) 909–918.
[23] E. Coutiño-Gonzalez, W. Baekelant, J.A. Steele, C.W. Kim, M.B.J. Roeffaers, J. Hofkens, Silver clusters in zeolites: from self-assembly to ground-breaking luminescent properties, Accounts Chem. Res. 50 (2017) 2353–2361.
[24] T. Altantzis, E. Coutino-Gonzalez, W. Baekelant, G.T. Martinez, A.M. Abakumov, G. V. Tendeloo, M.B.J. Roeffaers, S. Bals, J. Hofkens, Direct observation of luminescent silver clusters confined in faujasite zeolites, ACS Nano 10 (2016) 7604–7611.
[25] J.L. Cerrillo, A.E. Palomares, F. Rey, S. Valencia, M.B. Pérez-Gago, D. Villamón, L. Palou, Functional Ag-exchanged zeolites as biocide agents, ChemistrySelect 3 (2018) 4676–4682.
[26] S. Chen, J. Popovich, N. Iannuzo, S.E. Haydel, D.-K. Seo, Silver-ion-exchanged nanostructured zeolite X as antibacterial agent with superior ion release kinetics and efficacy against methicillin-resistant Staphylococcus aureus, ACS Appl. Mater. Interfaces 9 (2017) 39271–39282.
[27] K. Shimizu, K. Sawabe, A. Satsuma, Unique catalytic features of Ag nanoclusters for selective NOx reduction and green chemical reactions, Catal. Sci. Technol. 1 (2011) 331–341.

[28] R. Bartolomeu, A.N. Mendes, A. Fernandes, C. Henriques, P. da Costa, M.F. Ribeiro, NOx SCR with decane using Ag–MFI catalysts: on the effect of silver content and co-cation presence, Catal. Sci. Technol. 6 (2016) 3038–3048.
[29] K. Mathisen, M.H. Nilsen, C. Nordhei, D.G. Nicholson, Irreversible silver(I) interconversion in Ag:ZSM-5 and Ag:SAPO-5 by propene and hydrogen, J. Phys. Chem. C 116 (2012) 171–184.
[30] R. Bartolomeu, B. Azambre, A. Westermann, A. Fernandes, R. Bértolo, H. I. Hamoud, C. Henriques, P. Da Costa, F. Ribeiro, Investigation of the nature of silver species on different Ag-containing NOx reduction catalysts: on the effect of the support, Appl. Catal. B Environ. 150–151 (2014) 204–217.
[31] K.-i. Shimizu, K. Sugino, K. Kato, S. Yokota, K. Okumura, A. Satsuma, Reaction mechanism of H2-promoted selective catalytic reduction of NO with C3H8 over Ag−MFI zeolite, J. Phys. Chem. C 111 (2007) 6481–6487.
[32] H. Yang, C. Ma, X. Zhang, Y. Li, J. Cheng, Z. Hao, Understanding the active sites of Ag/zeolites and deactivation mechanism of ethylene catalytic oxidation at room temperature, ACS Catal. 8 (2018) 1248–1258.
[33] Y. Ono, T. Baba, Unique properties of silver cations in solid-acid catalysis by zeolites and heteropolyacids, Phys. Chem. Chem. Phys. 17 (2015) 15637–15654.
[34] A. Śrębowata, R. Baran, G. Słowik, D. Lisovytskiy, S. Dzwigaj, Influence of the postsynthesis preparation procedure on catalytic behaviour of Ag-loaded BEA zeolites in the hydrodechlorination of 1, 2-dichloroethane into value added products, Appl. Catal. B Environ. 199 (2016) 514–522.
[35] L. Zhang, Y. Xie, Y. Jiang, Y. Li, C. Wang, S. Han, H. Luan, X. Meng, F.-S. Xiao, Mn-promoted Ag supported on pure siliceous Beta zeolite (Ag/Beta-Si) for catalytic combustion of formaldehyde, Appl. Catal. B Environ. 268 (2020) 118461.
[36] K. Góra-Marek, K.A. Tarach, Z. Piwowarska, M. Łaniecki, L. Chmielarz, Ag-loaded zeolites Y and USY as catalysts for selective ammonia oxidation, Catal. Sci. Technol. 6 (2016) 1651–1660.
[37] Z. Qu, H. Wang, S. Wang, H. Cheng, Y. Qin, Z. Wang, Role of the support on the behavior of Ag-based catalysts for NH3 selective catalytic oxidation (NH3-SCO), Appl. Surf. Sci. 316 (2014) 373–379.
[38] Z. Wang, Q. Sun, D. Wang, Z. Hong, Z. Qu, X. Li, Hollow ZSM-5 zeolite encapsulated Ag nanoparticles for SO2-resistant selective catalytic oxidation of ammonia to nitrogen, Separ. Purif. Technol. 209 (2019) 1016–1026.
[39] N. Popovych, P. Kyriienko, S. Soloviev, R. Baran, Y. Millot, S. Dzwigaj, Identification of the silver state in the framework of Ag-containing zeolite by XRD, FTIR, photoluminescence, 109Ag NMR, EPR, DR UV-vis, TEM and XPS investigations, Phys. Chem. Chem. Phys. 18 (2016) 29458–29465.
[40] L. Zhang, H. He, Mechanism of selective catalytic oxidation of ammonia to nitrogen over Ag/Al2O3, J. Catal. 268 (2009) 18–25.
[41] M. Jabłońska, A.M. Beale, M. Nocuń, R. Palkovits, Ag-Cu based catalysts for the selective ammonia oxidation into nitrogen and water vapour, Appl. Catal. B Environ. 232 (2018) 275–287.
[42] S. Hinokuma, Y. Kawabata, S. Matsuki, H. Shimanoe, S. Kiritoshi, M. Machida, Local structures and catalytic ammonia combustion properties of copper oxides and silver supported on aluminum oxides, J. Phys. Chem. C 121 (2017) 4188–4196.
[43] M. Chebbi, B. Azambre, L. Cantrel, A. Koch, A combined DRIFTS and DR-UV–vis spectroscopic in situ study on the trapping of CH3I by silver-exchanged faujasite zeolite, J. Phys. Chem. C 120 (2016) 18694–18706.
[44] C. Shi, M. Cheng, Z. Qu, X. Bao, Investigation on the catalytic roles of silver species in the selective catalytic reduction of NOx with methane, Appl. Catal. B Environ. 51 (2004) 171–181.
[45] R. Jenkins, T.G. Fawcett, D.K. Smith, J.W. Visser, M.C. Morris, L.K. Frevel, JCPDS — international centre for diffraction data sample preparation methods in X-ray powder diffraction, Powder Diffr. 1 (2013) 51–63.
[46] G.H. Penner, W. Li, Silver-109 NMR spectroscopy of inorganic solids, Inorg. Chem. 43 (2004) 5588–5597.
[47] L. Simonelli, C. Marini, W. Olszewski, M. Ávila Pérez, N. Ramanan, G. Guilera, V. Cuartero, K. Klementiev, CLÆSS: the hard X-ray absorption beamline of the ALBA CELLS synchrotron, Cogent Phys. 3 (2016) 1231987.
[48] G. Guilera, F. Rey, J. Hernández-Fenollosa, J.J. Cortés-Vergaz, One body, many heads; the Cerberus of catalysis. A new multipurpose in-situ cell for XAS at ALBA, J. Phys. Conf. 430 (2013), 012057.
[49] B.N. Revel, M. Athena, ARTEMIS, HEPHAESTUS: data analysis for X-ray absorption spectroscopy using IFEFFIT, J. Synchrotron Radiat. 12 (2005) 537–541.
[50] F. Schuricht, W. Reschetilowski, Simultaneous selective catalytic reduction (SCR) of NOx and N2O over Ag/ZSM-5 – catalytic studies and mechanistic implications, Microporous Mesoporous Mater. 164 (2012) 135–144.
[51] R. Bartolomeu, R. Bértolo, S. Casale, A. Fernandes, C. Henriques, P. da Costa, F. Ribeiro, Particular characteristics of silver species on Ag-exchanged LTL zeolite in K and H form, Microporous Mesoporous Mater. 169 (2013) 137–147.
[52] C. Lamberti, C. Prestipino, S. Bordiga, A.N. Fitch, G.L. Marra, Characterization of isolated Ag cations in homoionic Ag-Y zeolites: a combined anomalous XRPD and EXAFS study, Nucl. Instrum. Methods Phys. Res. Sect. B Beam Interact. Mater. Atoms 200 (2003) 155–159.
[53] M. Moreno-González, A.E. Palomares, M. Chiesa, M. Boronat, E. Giamello, T. Blasco, Evidence of a Cu2+–alkane interaction in Cu-zeolite catalysts crucial for the selective catalytic reduction of NOx with hydrocarbons, ACS Catal. 7 (2017) 3501–3509.
[54] G. Agostini, S. Usseglio, E. Groppo, M.J. Uddin, C. Prestipino, S. Bordiga, A. Zecchina, P.L. Solari, C. Lamberti, From isolated Ag+ ions to aggregated Ag0 nanoclusters in silver-exchanged engelhard titanosilicate (ETS-10) molecular sieve: reversible behavior, Chem. Mater. 21 (2009) 1343–1353.
[55] C.-M. Lin, T.-L. Hung, Y.-H. Huang, K.-T. Wu, M.-T. Tang, C.-H. Lee, C.T. Chen, Y. Y. Chen, Size-dependent lattice structure of palladium studied by x-ray absorption spectroscopy, Phys. Rev. B 75 (2007) 125426.
[56] G. Agostini, R. Pellegrini, G. Leofanti, L. Bertinetti, S. Bertarione, E. Groppo, A. Zecchina, C. Lamberti, Determination of the particle size, available surface area, and nature of exposed sites for Silica−Alumina-supported Pd nanoparticles: a multitechnical approach, J. Phys. Chem. C 113 (2009) 10485–10492.
[57] G. Agostini, A. Piovano, L. Bertinetti, R. Pellegrini, G. Leofanti, E. Groppo, C. Lamberti, Effect of different face centered cubic nanoparticle distributions on particle size and surface area determination: a theoretical study, J. Phys. Chem. C 118 (2014) 4085–4094.
[58] L. Liu, M. Lopez-Haro, C.W. Lopes, C. Li, P. Concepcion, L. Simonelli, J.J. Calvino, A. Corma, Regioselective generation and reactivity control of subnanometric platinum clusters in zeolites for high-temperature catalysis, Nat. Mater. 18 (2019) 866–873.
[59] G.E. Pavlovskaya, C.F. Horton-Garcia, C. Dybowski, D.R. Corbin, T. Meersmann, Metallic clusters and color changes in silver-exchanged Zeolites: 109Ag solid state NMR and optical studies, J. Phys. Chem. B 108 (2004) 1584–1589.
[60] G. Xu, J. Ma, L. Wang, Z. Lv, S. Wang, Y. Yu, H. He, Mechanism of the H2 effect on NH3-selective catalytic reduction over Ag/Al2O3: kinetic and diffuse reflectance infrared fourier transform spectroscopy studies, ACS Catal. 9 (2019) 10489–10498.